Contribution from the Department of Chemistry,
Purdue University, West Lafayette, Indiana 47907

Mixed-Ligand Complexes of Tetracyanonickelate(III) and Dynamic Jahn-Teller Distortions of Hexacyanonickelate(III)

Yi Lai Wang, Mark W. Beach, Thomas L. Pappenhagen, and Dale W. Margerum*

Received May 24, 1988

Oxidation of $Ni^{II}(CN)_4^{2-}$ in aqueous solution gives *trans*-$Ni^{III}(CN)_4(H_2O)_2^-$, which has labile axial water molecules that are readily replaced by other ligands. Electron paramagnetic resonance (EPR) spectra of frozen aqueous solutions indicate a variety of tetragonally elongated complexes with two equivalent axial donors, where an increase in g_{av} values ($CN^- < NH_3 <$ imidazole $< N_3^- <$ pyridine $< CH_3CN < Cl^- < NCO^- < H_2O$) reflects a decrease in axial donor strength. Not all these complexes form in aqueous solution at room temperature, but five-line EPR spectra are seen for bis complexes of NH_3, imidazole, and pyridine. At 25 °C the values for the stepwise stability constants with pyridine are $K_1 \simeq 1 \times 10^5$ M^{-1} and $K_2 \simeq 4 \times 10^2$ M^{-1}. Excess cyanide gives $Ni^{III}(CN)_6^{3-}$, which has temperature-dependent EPR spectra in frozen aqueous solutions (−220 to −35 °C) due to dynamic Jahn-Teller distortions. Studies with $^{13}CN^-$ confirm the presence of six cyanides around Ni(III). The reduction potential for $Ni^{III}(CN)_4(H_2O)_2^-$ is 1.15 V (vs NHE). The complex decomposes with a first-order rate constant of 4.0×10^{-4} s^{-1} (pH 1-3, 25.0 °C, μ = 0.1, $\Delta H^* = 108$ kJ mol^{-1}, $\Delta S^* = 51$ J mol^{-1} K^{-1}). Base greatly accelerates this redox decomposition ($k_{obsd} = 0.45$ s^{-1}, −log [H^+] = 11.5, 25.0 °C, μ = 0.1, $\Delta H^* = 95$ kJ mol^{-1}, $\Delta S^* = 69$ J mol^{-1} K^{-1}). Nickel(III) oxidizes cyanide to cyanate, and the stoichiometry of the decomposition is $8Ni^{III}(CN)_4(H_2O)_2^- + 10OH^- \rightarrow 7Ni^{II}(CN)_4^{2-} + 4OCN^- + Ni(OH)_2 + 20H_2O$.

Introduction

Aqueous solutions of $Ni^{II}(CN)_4^{2-}$ can be chemically or electrochemically oxidized to form *trans*-$Ni^{III}(CN)_4(H_2O)_2^-$ (structure I) as reported earlier.[1] Although the reduction potential for this

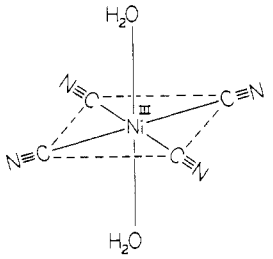

I

couple is greater than 1 V, the redox decomposition of the complex does not occur by the oxidation of water. Our stoichiometric measurements show that CN^- is oxidized to OCN^- as Ni(III) is reduced to Ni(II).

The rate of decomposition of $Ni^{III}(CN)_4(H_2O)_2^-$ in acid increases with the free HCN concentration, which in turn depends on the rate of acid dissociation[2] of $Ni^{II}(CN)_4^{2-}$. Hence, the observed rate constant for the loss of Ni(III) depends upon the initial concentration of $Ni^{II}(CN)_4^{2-}$ and the efficiency of its oxidation to Ni(III). A bulk electrolysis column[3] is a more convenient way to prepare solutions of $Ni^{III}(CN)_4(H_2O)_2^-$ than chemical oxidation with monopersulfate or lead dioxide. However, the efficiency of electrochemical oxidation is poor. We find that hypochlorous acid is advantageous because it gives a rapid, quantitative oxidation of Ni(II) to Ni(III) and it also destroys any free cyanide (or HCN) in the solution.[4] Different modes of preparation of $Ni^{III}(CN)_4(H_2O)_2^-$ and the effects of pH and excess $Ni^{II}(CN)_4^{2-}$, HCN, OCN^-, and H_2O_2 are compared in order to establish the decomposition rate dependence. The half-life of the $Ni^{III}(CN)_4(H_2O)_2^-$ complex itself is 28 min (at 25 °C, pH 1-3) rather than 11 min as reported previously.[1]

The axial water molecules in the Ni(III) complex are rapidly substituted by other ligands to form a variety of mixed-ligand complexes. Large hyperfine coupling constants cause dramatic splittings of both frozen and room-temperature EPR spectra. Complexes of *trans*-$Ni^{III}(CN)_4L_2^-$ form in aqueous solution where L = NH_3, imidazole, or pyridine, whereas only mono adducts could be found for these ligands with Ni^{III}(peptide) complexes at room temperature.[5] Studies with pyridine permit stability constants to be estimated for the mono- and bis(pyridine) complexes.

Experimental Section

Stock solutions of $Ni(ClO_4)_2$ were prepared from the reaction of $NiCO_3$ and $HClO_4$ and were standardized by titration with EDTA to a murexide end point. The purity of NaCN (Aldrich) was verified by argentimetry in the presence of iodide. Isotopically enriched $Na^{13}CN$ (99% enriched carbon-13) and $NaC^{15}N$ (99% enriched nitrogen-15) from Strohler Isotope Chemicals (Waltham, MA) were used as received. Cyanide solutions were used within 48 h of preparation to minimize decomposition. Isotopically enriched nickel-61 metal (88.9% nickel-61) from Oak Ridge National Laboratory (Oak Ridge, TN) was dissolved in dilute nitric acid. Solutions of $Ni(^{13}CN)_4^{2-}$, $Ni(C^{15}N)_4^{2-}$, and $^{61}Ni(CN)_4^{2-}$ were prepared by reaction of 1.0×10^{-3} M $Ni(ClO_4)_2$ with 4.05×10^{-3} M CN^-. Crystalline $Na_2Ni(CN)_4$ and $K_2Ni(CN)_4$ were prepared as described previously.[6] All nickel(II) solutions were used within 24 h of preparation.

trans-Diaquatetracyanonickelate(III) solutions were prepared by electrochemical oxidation of the corresponding nickel(II) complex with a flow-through bulk electrolysis column.[3] Prior to electrolysis the $Ni^{II}(CN)_4^{2-}$ solutions were adjusted to pH values between 9.3 and 10.0, and the ionic strength was adjusted to 0.10 with $NaClO_4$. Potentials between 1.00 and 1.20 V (vs a Ag/AgCl reference electrode) and a flow rate of 1.1 mL min^{-1} were used for the bulk electrolysis. The electrolysis increases the acidity of the solution to pH 4. Typical yields of $Ni^{III}(CN)_4(H_2O)_2^-$ ranged from 30 to 60%. Hypochlorous acid, which was prepared from sodium hypochlorite (10% solution, Baker), Oxone ($2KHSO_5 \cdot KHSO_4 \cdot K_2SO_4$, Du Pont Co.), and lead dioxide (Fisher Scientific) were used to oxidized $Ni(CN)_4^{2-}$ solutions. A 10-fold excess of the oxidant to $Ni^{II}(CN)_4^{2-}$ was used. The nickel(III) solutions were kept in dilute $HClO_4$ (pH 2-3) to reduce the rate of redox decomposition. Mixed-ligand complexes were prepared by reaction of $Ni^{III}(CN)_4(H_2O)_2^-$ and excess ligand, followed by immediate measurement of the EPR signal for aqueous studies, or by quenching the sample (within 15 s) in liquid nitrogen for frozen samples.

Electron paramagnetic resonance spectra were obtained with a Varian E-109 X-band EPR spectrometer modulated at 100 kHz. A Varian E-231 variable-temperature cavity and a Varian E-238 variable-temperature controller were used to control the temperature of frozen samples. Liquid-helium temperatures were controlled with an Air Products APD-B variable-temperature controller.

Room-temperature EPR spectra were obtained with a Varian E-238 multipurpose cavity and either a thin (0.1 mm) quartz cell or a thin quartz cell equipped with a two-jet tangential mixer (Wilmad). Rapid-scan EPR experiments were performed with a Varian E-271A rapid-scan

(1) Pappenhagen, T. L.; Margerum, D. W. *J. Am. Chem. Soc.* **1985**, *107*, 4576-4577.
(2) Kolski, G. B.; Margerum, D. W. *Inorg. Chem.* **1968**, *7*, 2239-2243.
(3) Neubecker, T. A.; Kirskey, S. T., Jr.; Margerum, D. W. *Inorg. Chem.* **1979**, *18*, 444-448.
(4) Eden, E. G.; Hampson, B. L.; Wheatland, A. B. *J. Soc. Chem. Ind., London* **1950**, *69*, 244-249.
(5) Murray, C. K.; Margerum, D. W. *Inorg. Chem.* **1982**, *21*, 3501-3506.
(6) Fernelius, W. C., Ed. *Inorganic Synthesis*; McGraw-Hill: New York, 1946; Vol. 2, pp 227-228.

0020-1669/88/1327-4464$01.50/0

Table I. Calculated g Values and Hyperfine Coupling Constants (A, G) for Nickel(III) Tetracyano Complexes in Frozen Aqueous Solutions at −150 °C and a Microwave Frequency of 9.08 GHz

	g_{xx}	g_{yy}	g_{zz}	g_{av}	A_{xx}	A_{yy}	A_{zz}	ref
$Ni^{III}(CN)_4(H_2O)_2^-$	2.198	2.198	2.007	2.134				*a*
$Ni^{III}(CN)_4(NCO)_2^{3-}$	2.165	2.165	2.008	2.113	16.0	16.0	18.5	*b*
$Ni^{III}(CN)_4(Cl)_2^{3-}$	2.161	2.161	2.008	2.110	9.5	9.5	33.6	*b*
$Ni^{III}(CN)_4(NCCH_3)_2^-$	2.145	2.145	2.007	2.099	20.6	20.6	24.5	*b*
$Ni^{III}(CN)_4(py)_2^-$	2.137	2.137	2.009	2.094	19.8	19.8	25.3	*b*
$Ni^{III}(CN)_4(N_3)_2^{3-}$	2.132	2.132	2.008	2.091	13.0	13.0	16.2	*b*
$Ni^{III}(CN)_4(imid)_2^-$	2.125	2.125	2.008	2.086	22.1	22.1	27.1	*b*
$Ni^{III}(CN)_4(NH_3)_2^-$	2.116	2.116	2.009	2.080	18.0	18.0	24.0	*a*
$Ni^{III}(CN)_6^{3-}$ [c]	2.081	2.081	2.010	2.057				*a*
$Ni^{III}(CN)_4(bpy)^-$	2.039	2.039	2.138	2.072	14.3	14.3	1	*b*

[a] Reference 1. [b] This work. [c] −190 °C.

unit interfaced to a 8080A-based microcomputer, a controller/function generator combination, and the Varian E-109 spectrometer.[7] A Varian E-935 data acquisition system was used to obtain kinetic measurements.

Hyperfine coupling constants (A), broadening parameters (W), and g values were determined from a computer-generated spectral-matching procedure described elsewhere.[8,9] EPR spectra of frozen samples of the tetracyano complexes were simulated by assuming equivalent equatorial axes ($g_{xx} = g_{yy}$). Better fits were not obtained with different equatorial g values. The g and A values are initially estimated by inspection and refined by the simulation procedure to line up the peaks. The broadening parameters are then introduced to match the simulated and experimental EPR spectra. The magnetic field was calibrated relative to α,α'-diphenyl-β-picrylhydrazyl (DPPH).

Ultraviolet spectra were recorded on a Perkin-Elmer 320 spectrophotometer, equipped with a P-E 3600 Data Station. The decomposition kinetics of $Ni^{III}(CN)_4(H_2O)_2^-$ were measured under pseudo-first-order conditions with this instrument or by stopped-flow methods at 25.0 ± 0.1 °C. A Dionex-Durrum Model D-110 stopped-flow spectrometer interfaced to a Hewlett-Packard 2100 computer was used as well as a Hi-Tech Scientific Model SFL-43 mixing module attached by fiber optics to a Durrum D-110 monochromator and interfaced to a Zenith 151 CPU with a Metrabyte DASH-16 A/D interface. The decomposition of nickel(III) was followed at 234 nm, where $Ni^{II}(CN)_4^{2-}$ has little absorbance. The decomposition of mixed-ligand complexes of pyridine and imidazole were monitored at room temperature by their EPR signals at 3145 and 3205 G, respectively. The decomposition of $Ni^{III}(CN)_4(H_2O)_2^-$ was measured under similar reaction conditions (monitored at 3115 G) for comparison.

Cyclic voltammetry was performed with a three-electrode system that employed a Ag/AgCl (3 M NaCl, $E°$ = 0.194 V vs NHE) reference electrode, a platinum-wire auxiliary electrode, and either a glassy-carbon or carbon-paste working electrode. A Bioanalytical Systems, Inc., BAS 100 electrochemical analyzer was used to generate voltammograms.

A Wescan Model 266 ion analyzer with a conductivity detector was used to separate and determine cyanate ion. A resin-based anion-exchange column (Wescan Anion/R, 269-029) suitable for a pH range of 2–13 was used. The mobile phase contained 1×10^{-3} M potassium hydrogen phthalate (pH adjusted to 5.5 with NaOH). The chromatographic parameters were as follows: flow rate 2.0 mL/min; sensitivity range 1; sample loop 0.1 mL. The cyanate peak was identified by its retention time (about 4 min) and the increase of the peak height upon adding potassium cyanate to the sample solution. A standard addition method was used to determine the concentration of the cyanate ion.

An Orion 601A pH meter with an Orion combination pH electrode was used for pH measurements. The pH values were measured to within ±0.01 unit and were corrected to −log [H^+] values at 25.0 °C and μ = 0.1 M based on electrode calibrations by titration of standard $HClO_4$ (0.005 M) with standard NaOH (0.10 M) solutions.

Results and Discussion

$Ni^{III}(CN)_4(H_2O)_2^-$ Preparation and Electrode Potential. The $Ni^{III}(CN)_4(H_2O)_2^-$ complex is generated by oxidation of $Ni^{II}(CN)_4^{2-}$ either electrochemically with a flow-through bulk electrolysis column or chemically with hypochlorous acid (NaOCl in 0.1–0.001 M $HClO_4$), Oxone (pH 1–10), or lead dioxide (pH 2–5). Bulk electrolysis of $Ni^{II}(CN)_4^{2-}$ has low efficiency (<60% at 1.20 V vs Ag/AgCl) but does not introduce spectral or chemical interferences. Chemical oxidation has a higher efficiency. With hypochlorous acid the oxidation of $Ni^{II}(CN)_4^{2-}$ is nearly complete and spectral interference is avoided because OCl^- (λ_{max} at 292 nm, ϵ = 350 M^{-1} cm^{-1}) and HOCl (λ_{max} at 233 nm, ϵ = 97 M^{-1} cm^{-1}) both have very small absorbance in the UV region compared to $Ni^{II}(CN)_4^{2-}$ ($\epsilon_{267} = 1.16 \times 10^4$ M^{-1} cm^{-1}, $\epsilon_{285} = 4.63 \times 10^3$ M^{-1} cm^{-1})[10] and $Ni^{III}(CN)_4(H_2O)_2^-$ ($\epsilon_{255} = 1.19 \times 10^4$ M^{-1} cm^{-1}). It appears that chlorine, which is in equilibrium with HOCl as shown in eq 1 ($K = 1.7 \times 10^3$ M^{-2}),[11] may play a role in the

$$HOCl + H^+ + Cl^- \rightleftarrows Cl_2 + H_2O \quad (1)$$

oxidation of $Ni^{II}(CN)_4^{2-}$ to $Ni^{III}(CN)_4(H_2O)_2^-$. The hypochlorite solution contains an equal concentration of chloride, and the more rapid oxidation of $Ni^{II}(CN)_4^{2-}$ to $Ni^{III}(CN)_4(H_2O)_2^-$ as the acid concentration increases is attributed to oxidation by Cl_2.

The reduction potential of $Ni^{III}(CN)_4(H_2O)_2^-$ is 1.15 ± 0.02 V vs NHE at 25.0 °C, μ = 0.1. The value is independent of acidity from pH 2 to 7. This is 0.33 V higher than the value for the $Ni^{III,II}(H_{-2}Aib_3)^{0,-}$ couple ($H_{-2}Aib_3$ is the doubly deprotonated tripeptide of α-aminoisobutyric acid)[12] and is 0.12 V higher than the value for $Ni^{III,II}(cyclam)^{3+,2+}$ (cyclam is 1,4,8,11-tetraazacyclotetradecane).[13] This increase in the nickel(III,II) potential indicates either a decrease in the relative stability of the nickel(III) complex or an increase in the relative stability of the corresponding nickel(II) complex as compared with the Aib_3 or cyclam complexes. The deprotonated-N(peptide) groups in the Aib_3 complex are very strong donors and help to stabilize this Ni(III) complex. Cyanide ion appears to be a weaker donor for Ni(III) than the deprotonated-N(peptide) group but is similar to or slightly lower in strength than secondary amines. The favorable stability of the $Ni^{II}(CN)_4^{2-}$ complex[2] may contribute to the high electrode potential of the $Ni^{III}(CN)_4(H_2O)_2^-/Ni^{II}(CN)_4^{2-}$ couple. The temperature dependence of the potentials for Ni(III,II) peptide couples[14] shows that two axial water molecules also are released in the reduction of these Ni(III) complexes.

EPR Spectra. The frozen aqueous glass EPR spectrum of $^{61}Ni^{III}(CN)_4(H_2O)_2^-$ was reported previously.[1] It shows a quartet in the $g_\parallel$ region as expected from the ^{61}Ni nucleus ($I = {}^3/_2$), and the axial hyperfine coupling constant ($A_\parallel$ = 43.2 G) is similar to a value of 45.7 G found for the $^{61}Ni(H_{-2}Aib_3)(H_2O)_2$ complex.[15] The unpaired electron is associated primarily with the nickel atom. No noticeable $g_\perp$ splitting is observed, and $A_\perp$ is estimated to be less than 8 G. Both spectra have $g_\perp > g_\parallel$, which indicates the complexes have tetragonally elongated geometries.[8,16,17] These g values (Table I) agree well with the spectrum reported for the

(7) Jacobs, S. A.; Kramer, G. W.; Santini, R. E.; Margerum, D. W. *Anal. Chim. Acta* **1984**, *157*, 117–124.
(8) Pappenhagen, T. L.; Kennedy, W. R.; Bowers, C. P.; Margerum, D. W. *Inorg. Chem.* **1985**, *24*, 4356–4362.
(9) Toy, A. D.; Chaston, S. H. H.; Pilbrow, J. R.; Smith, T. D. *Inorg. Chem.* **1971**, *10*, 2219–2226.
(10) Crouse, W. C.; Margerum, D. W. *Inorg. Chem.* **1974**, *13*, 1437–1443.
(11) Eigen, M.; Kustin, K. *J. Am. Chem. Soc.* **1962**, *84*, 1355–1361.
(12) Owens, G. D.; Phillips, D. A.; Czarnecki, J. J.; Raycheba, J. M. T.; Margerum, D. W. *Inorg. Chem.* **1984**, *23*, 1345–1353.
(13) Kumar, K.; Rotzinger, F. P.; Endicott, J. F. *J. Am. Chem. Soc.* **1983**, *105*, 7064–7074.
(14) Youngblood, M. P.; Margerum, D. W. *Inorg. Chem.* **1980**, *19*, 3068–3072.
(15) Pappenhagen, T. L.; Margerum, D. W., to be submitted for publication.
(16) Lappin, A. G.; Murray, C. K.; Margerum, D. W. *Inorg. Chem.* **1978**, *17*, 1630–1634.
(17) Jacobs, S. A.; Margerum, D. W. *Inorg. Chem.* **1984**, *23*, 1195–1201.

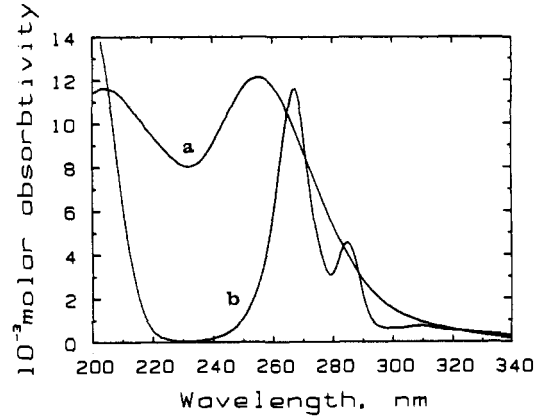

Figure 1. UV spectra of tetracyanonickelate complexes: (a) $Ni^{III}(CN)_4(H_2O)_2^-$ in 0.1 M $HClO_4$; (b) $Ni^{II}(CN)_4^{2-}$ in 0.1 M $NaClO_4$.

γ-irradiation of $Ni^{II}(CN)_4^{2-}$ in frozen aqueous solution.[18]

The narrowness and symmetry of the $g_\perp$ region for the EPR spectrum of I indicate the presence of four equivalent equatorial donors. A single peak in the $g_\parallel$ region demonstrates that the axial positions are occupied by donor atoms with no nuclear spin ($I = 0$). This would be the case for water molecules or carbon-bound CN^-. The lack of additional $g_\parallel$ splitting in the ^{13}C-enriched cyano complex, $Ni^{III}(^{13}CN)_4(H_2O)_2^-$, shows that the two axial positions are indeed occupied by water molecules.

The EPR spectra of frozen solutions that contain the $Ni^{III}(^{13}CN)_4(H_2O)_2^-$ complex also show no evidence of $g_\perp$ ^{13}C splitting from the equatorial cyanides. This is very interesting in light of the fact that a $g_\perp$ ^{13}C hyperfine splitting of 92 G is observed from axial cyanides in the hexacyano complex. Axial substitution of the water molecules by donor groups with a nuclear spin causes strong splitting of $g_\parallel$ and often splits $g_\perp$ as well.[8,16] In the case of equatorial $^{13}CN^-$ groups, the lack of splitting indicates a negligible interaction between their sp donor orbitals and the x and y components of the nickel(III) d_{z^2} (i.e. $d_{z^2-x^2-y^2}$) orbital, which contains the unpaired electron. Similar behavior is observed with nickel(III) peptide complexes where equatorial nitrogens do not cause $g_\perp$ splitting.[8,16]

The g_{av} value of 2.142 for the $Ni^{III}(CN)_4(H_2O)_2^-$ in the frozen state is less than the g_{av} values of 2.17–2.20 for nickel(III) peptide complexes[16,19] or for $Ni^{III}(cyclam)(H_2O)_2^{3+}$, where g_{av} is 2.157.[20] Studies with nickel(III) peptides show that the g_{av} value tends to increase as the strength of the equatorial donor groups increase to give a more tetragonally distorted complex.[16] As the equatorial donor strength increases, there is an increase in the $g_\perp$ (g_{xx}, g_{yy}) values. Thus, EPR spectra indicate that cyanide is a weaker donor with nickel(III) than is the deprotonated peptide (N(−)) or secondary amine nitrogens. In contrast, EPR studies of cyano-substituted nickel(III) tripeptide complexes show cyanide to be a slightly stronger donor than primary amine nitrogens.[15] The overall series for ligand donor strength is

$$N(-) \gg >NH \geq CN^- \geq -NH_2$$

UV Spectrum. The UV spectrum of $Ni^{III}(CN)_4(H_2O)_2^-$ (Figure 1) has a broad peak at 255 nm.[1] The $Ni^{II}(CN)_4^{2-}$ spectrum, also given in Figure 1 for comparison, has absorption peaks at 267, 285, and 310 nm. An indirect method was used to determine the ϵ values of $Ni^{III}(CN)_4(H_2O)_2^-$ prepared electrochemically. First, the molar absorptivity at 234 nm was determined by spectrophotometric titration with $Fe(CN)_6^{4-}$ in 0.10 M $HClO_4$. This permitted calculation of the concentration of the nickel(III) cyano complex. The total nickel(II) concentration, $[Ni^{II}(CN)_4^{2-}]_T$, was determined by the addition of an excess of ascorbic acid to the nickel(III) solution, which resulted in the rapid reduction of all nickel(III) to $Ni^{II}(CN)_4^{2-}$. The concentration of $Ni^{II}(CN)_4^{2-}$ in the original nickel(III) solution is then the difference between $[Ni^{II}(CN)_4^{2-}]_T$ and $[Ni^{III}(CN)_4(H_2O)_2^-]$. The molar absorptivity at 255 nm is calculated from the ratio of the corrected absorbances at the two wavelengths. Direct measurements of ϵ values were taken for $Ni^{III}(CN)_4(H_2O)_2^-$ prepared with HOCl, because HOCl has negligible absorption in this spectral region and the oxidation of $Ni^{II}(CN)_4^{2-}$ to $Ni^{III}(CN)_4(H_2O)_2^-$ is complete. The ϵ_{255} values calculated from both methods agree, and the average value is $(1.19 \pm 0.05) \times 10^4$ M^{-1} cm^{-1}.

Table II. Yield of $Ni^{II}(CN)_4^{2-}$ in the Decomposition of $Ni^{III}(CN)_4(H_2O)_2^-$[a]

−log [H^+]	% yield of $Ni^{II}(CN)_4^{2-}$	medium
5.0	73	0.1 M $HOAc/OAc^-$
6.0	79	0.1 M phosphate
7.5	81	0.1 M phosphate
9.5	86	0.1 M carbonate
11.7	85	5 mM OH^-

[a] $[Ni^{III}(CN)_4(H_2O)_2^-]_{initial} = 3.23 \times 10^{-5}$ M; $[Ni^{II}(CN)_4^{2-}]_{initial} = 1.60 \times 10^{-5}$ M.

Table III. Redox Decomposition Rate Constants for $Ni^{III}(CN)_4(H_2O)_2^-$ in Acid and Base[a]

−log [H^+]	$10^3 k_{obsd}$, s^{-1} [b]	$10^3 k_{obsd}$, s^{-1} [c]	−log [H^+]	$10^3 k_{obsd}$, s^{-1} [b]	$10^3 k_{obsd}$, s^{-1} [c]
0.0[d]	0.50 ± 0.03	1.4 ± 0.1	5.00	0.63 ± 0.05	3.6 ± 0.5
1.00[e]	0.39 ± 0.02	0.88 ± 0.06	6.84	1.4 ± 0.1	4.2 ± 0.2
2.00	0.40 ± 0.03	1.1 ± 0.3	10.00	1400 ± 100	
3.00	0.41 ± 0.02	1.4 ± 0.3	10.21		74 ± 4
4.00	0.44 ± 0.02	2.7 ± 0.5	11.50	36000 ± 3000	450 ± 10

[a] $\mu = 0.1$ ($NaClO_4$) except where noted; 25.0 °C. [b] $Ni^{III}(CN)_4(H_2O)_2^-$ prepared from HOCl oxidation; $[Ni^{III}(CN)_4(H_2O)_2^-] = 5 \times 10^{-5}$ M; $[HOCl] = 5 \times 10^{-4}$ M. [c] $Ni^{III}(CN)_4(H_2O)_2^-$ prepared by bulk electrolysis (1.00 V vs Ag/AgCl); $[Ni^{III}(CN)_4(H_2O)_2^-] = 3 \times 10^{-5}$ M. [d] $\mu = 1.0$ (1.0 M $HClO_4$). [e] $\mu = 0.2$ (0.1 M $HClO_4$, 0.1 M $NaClO_4$).

Stoichiometry of the Decomposition. Although $Ni^{III}(CN)_4(H_2O)_2^-$ has sufficient potential to oxidize water during its decomposition, this does not occur. Instead, the $Ni^{III}(CN)_4(H_2O)_2^-$ oxidizes part of its cyanide to cyanate. This is evidenced by (1) the detection of cyanate ion (by an ion chromatographic method) in the solution after the $Ni^{III}(CN)_4(H_2O)_2^-$ has decomposed and (2) the recovery of only a 71–86% yield of $Ni^{II}(CN)_4^{2-}$ in the pH range from 5 to 11.5 after the decomposition (Table II). If $Ni^{III}(CN)_4(H_2O)_2^-$ decomposed via water oxidation to oxygen, the recovery of $Ni^{II}(CN)_4^{2-}$ would be 100% in base. The possibility that water is oxidized to hydrogen peroxide, which then oxidizes cyanide to cyanate, can be ruled out because of the slow rate of the oxidation of cyanide by H_2O_2 (rate constant 1.5×10^{-3} M^{-1} s^{-1}).[21] We also find that H_2O_2 is oxidized by $Ni^{III}(CN)_4(H_2O)_2^-$ with a second-order rate constant of 600 ± 100 M^{-1} s^{-1}. Had hydrogen peroxide been produced, it would have been oxidized to oxygen by $Ni^{III}(CN)_4(H_2O)_2^-$ before it could oxidize cyanide to cyanate, and the recovery of $Ni^{II}(CN)_4^{2-}$ would still be 100%. The less than 100% recovery of $Ni^{II}(CN)_4^{2-}$ in base shows that $Ni^{III}(CN)_4(H_2O)_2^-$ oxidizes some of the cyanide. The amount of cyanate ion found in the solution corresponds to half of the concentration of $Ni^{III}(CN)_4(H_2O)_2^-$ originally present. This is expected, because oxidation of cyanide to cyanate requires two electrons. Equation 2 gives the stoichiometry of the decomposition

$$8Ni^{III}(CN)_4(H_2O)_2^- + 10OH^- \rightarrow 7Ni^{II}(CN)_4^{2-} + Ni(OH)_2 + 4OCN^- + 20H_2O \quad (2)$$

of $Ni^{III}(CN)_4(H_2O)_2^-$, based on the above evidence. According to eq 2, 87.5% of the $Ni^{II}(CN)_4^{2-}$ should be recovered in base. Below pH 8, however, the re-formation of $Ni^{II}(CN)_4^{2-}$ ($\log \beta_4 = 30$)[2] is less favorable as the concentration of CN^- is reduced due to HCN formation ($pK_a = 9.01$, $\mu = 0.1$).[22a] Hence, the lower

(18) Symons, M. C. R.; Aly, M. M.; West, P. X. *J. Chem. Soc., Dalton Trans.* **1979**, 1744–1748.
(19) Subak, E. J.; Loyola, V. M.; Margerum, D. W. *Inorg. Chem.* **1985**, *24*, 4350–4356.
(20) Haines, R. I.; McAuley, A. *Inorg. Chem.* **1980**, *19*, 719–723.
(21) Mason, O. *J. Chem. Soc.* **1907**, *91*, 1449–1474.

Table IV. Rate Constants for the Decomposition of $Ni^{III}(CN)_4(H_2O)_2^-$ with Added Hydrogen Cyanide[a,b]

$10^3[CN^-]$ added, M	10^3k_{obsd}, s^{-1}	$10^3[CN^-]$ added, M	10^3k_{obsd}, s^{-1}
0	1.42 ± 0.01	0.20	2.25 ± 0.02
0.05	1.58 ± 0.01	0.29	2.50 ± 0.02
0.10	1.89 ± 0.01		

[a] $[Ni^{III}(CN)_4(H_2O)_2^-] = 8 \times 10^{-5}$ M; $[H^+] = 0.01$ M; $\mu = 0.1$ ($NaClO_4$); 25.0 °C. [b] The resolved second-order rate constant is 3.8 ± 0.8 M^{-1} s^{-1}.

Table V. Observed Rate Constants for the Acid Decomposition of $Ni^{III}(CN)_4(H_2O)_2^-$ with Additional $Ni^{II}(CN)_4^{2-}$ [a]

$10^3[Ni^{II}(CN)_4^{2-}]$, M	10^3k_{obsd}, s^{-1}	$10^3[Ni^{II}(CN)_4^{2-}]$, M	10^3k_{obsd}, s^{-1}
0.12	1.49 ± 0.01	0.42	3.32 ± 0.03
0.22	2.19 ± 0.01	0.52	3.62 ± 0.03
0.32	2.83 ± 0.02		

[a] $[Ni^{III}(CN)_4(H_2O)_2^-] = 8 \times 10^{-5}$ M; $[H^+] = 0.01$ M; $\mu = 0.1$ ($NaClO_4$); 25.0 °C.

Table VI. Dependence of the Decomposition Rate Constant of $Ni^{III}(CN)_4(H_2O)_2^-$ on [Cyanate][a,b]

$10^3[OCN^-]_T$, M	10^3k_{obsd}, s^{-1}	$10^3[OCN^-]_T$, M	10^3k_{obsd}, s^{-1}
0	2.24 ± 0.05	7.8	3.86 ± 0.05
1.2	2.50 ± 0.04	11.8	4.77 ± 0.07
2.3	2.94 ± 0.02	15.5	5.37 ± 0.09
3.9	3.20 ± 0.04		

[a] $[Ni^{III}(CN)_4(H_2O)_2^-] = 3 \times 10^{-5}$ M; −log $[H^+]$ = 4.0 (0.1 M acetate); $\mu = 0.1$ ($NaClO_4$); 25.0 °C. [b] The resolved second-order rate constant is 0.20 ± 0.01 M^{-1} s^{-1}.

recovery of $Ni^{II}(CN)_4^{2-}$ at pH 5.0–7.5 in Table II is expected.

Kinetics of the Decomposition in Acid. Despite its high reduction potential (1.15 V vs NHE), the $Ni^{III}(CN)_4(H_2O)_2^-$ complex is moderately stable in acidic solutions. The half-life of $Ni^{III}(CN)_4(H_2O)_2^-$ is 28 min at pH 2 and changes little from pH 0 to 5. The observed first-order rate constants are listed in Table III as a function of pH for $Ni^{III}(CN)_4(H_2O)_2^-$ prepared by both HOCl oxidation and bulk electrolysis.

The decomposition of $Ni^{III}(CN)_4(H_2O)_2^-$ is slower in acid when it is prepared with HOCl than when it is prepared by bulk electrolysis. An additional function of hypochlorous acid is to scavenge any free cyanide, because HOCl rapidly reacts with hydrogen cyanide to form cyanate.[4] For bulk-electrolyzed $Ni^{III}(CN)_4(H_2O)_2^-$, the oxidation efficiency is low and some $Ni^{II}(CN)_4^{2-}$ is left in solution. This $Ni^{II}(CN)_4^{2-}$ will decompose in acid to give HCN and Ni^{2+}.[2,10] Free HCN increases the decomposition rate of $Ni^{III}(CN)_4(H_2O)_2^-$, as indicated in Table IV. A second-order rate constant of 3.8 ± 0.8 M^{-1} s^{-1} is measured for the redox reaction between HCN and $Ni^{III}(CN)_4(H_2O)_2^-$. When additional $Ni^{II}(CN)_4^{2-}$ is added to a solution of $Ni^{III}(CN)_4(H_2O)_2^-$, the decomposition rate of $Ni^{III}(CN)_4(H_2O)_2^-$ also increases (Table V). This could be due either to $Ni^{II}(CN)_4^{2-}$ decomposition in acid (5.0×10^{-4} s^{-1} in 0.01 M $[H^+]$ to form HCN and Ni^{2+}) or to a direct reaction between $Ni^{III}(CN)_4(H_2O)_2^-$ and $Ni^{II}(CN)_4^{2-}$.

After HOCl oxidation of HCN, there is a possibility that the cyanate product might also reduce $Ni^{III}(CN)_4(H_2O)_2^-$. There is also a subsequent much slower reaction of HOCl and cyanate to form carbonate and nitrogen gas.[23] Cyanate ions accelerate the decomposition of $Ni^{III}(CN)_4(H_2O)_2^-$ (Table VI). The second-order rate constant for the cyanate–$Ni^{III}(CN)_4(H_2O)_2^-$ reaction is 0.20 ± 0.01 M^{-1} s^{-1}. Hence, this reaction is negligible at the concentration levels of OCN^- produced in the kinetic studies of the decomposition of $Ni^{III}(CN)_4(H_2O)_2^-$. The oxidation of cyanate could occur by an inner-sphere pathway. Nevertheless, an EPR spectrum of $Ni^{III}(CN)_4(NCO)_2^{3-}$ is found with axial cyanates coordinated through the nitrogen atoms in frozen aqueous solution.

Since HOCl acts both as a scavenger of any free HCN and as an efficient oxidant for the quantitative oxidation of $Ni^{II}(CN)_4^{2-}$ to $Ni^{III}(CN)_4(H_2O)_2^-$, we believe that the HOCl preparation gives more reliable values of the observed rate constants (Table III) for the decomposition of $Ni^{III}(CN)_4(H_2O)_2^-$ in acidic solution.

No $Ni^{III}(CN)_4(H_2O)_2^-$ is observed when H_2O_2 is mixed with $Ni^{II}(CN)_4^{2-}$ in acid, despite the favorable difference in potential (0.61 V at standard conditions) for this reaction. On the other hand, the rate of loss of $Ni^{III}(CN)_4(H_2O)_2^-$ increases when hydrogen peroxide is present (Table VII). A second-order rate constant of (6 ± 1) × 10^2 M^{-1} s^{-1} is found when H_2O_2 acts as a reducing agent. The reduction potential for the O_2/H_2O_2 couple[24] is 0.695 V, which is 0.45 V lower than the $E°$ value for the $Ni^{III}(CN)_4(H_2O)_2^-/Ni^{II}(CN)_4^{2-}$ couple. The possibility of the catalytic decomposition of H_2O_2 by $Ni^{II}(CN)_4^{2-}$ is ruled out because no oxygen is released when $Ni^{II}(CN)_4^{2-}$ is added to an acidic 0.1 M H_2O_2 solution (in 0.1 M $HClO_4$).

Table VII. Observed Rate Constants for the Reaction of $Ni^{III}(CN)_4(H_2O)_2^-$ with Hydrogen Peroxide[a,b]

$10^3[H_2O_2]$, M	k_{obsd}, s^{-1}	$10^3[H_2O_2]$, M	k_{obsd}, s^{-1}
1.19	0.85 ± 0.09	4.78	3.7 ± 0.2
1.79	1.09 ± 0.05	7.16	5.1 ± 0.4
2.38	3.04 ± 0.09		

[a] $[Ni^{III}(CN)_4(H_2O)_2^-] = 3 \times 10^{-5}$ M; $[H^+] = 0.01$ M; $\mu = 0.1$ ($NaClO_4$); 25.0 °C. [b] The resolved second-order rate constant is (6 ± 1) × 10^2 M^{-1} s^{-1}.

Table VIII. Temperature Dependence and Activation Parameters for the Acid and Base Decomposition of $Ni^{III}(CN)_4(H_2O)_2^-$

	−log $[H^+]$			
	2.0[a]		11.7[b]	
	temp, °C	10^3k_{obsd}, s^{-1}	temp, °C	k_{obsd}, s^{-1}
	11.6	0.039 ± 0.003	5.0	0.030 ± 0.001
	25.0	0.40 ± 0.2	10.0	0.061 ± 0.001
	35.7	1.59 ± 0.07	15.0	0.128 ± 0.001
	42.2	3.7 ± 0.4	20.0	0.247 ± 0.002
			25.0	0.51 ± 0.01
			30.0	0.99 ± 0.01
ΔH^*, kJ mol^{-1}	108 ± 4		95 ± 1	
ΔS^*, J mol^{-1} K^{-1}	52 ± 3		69 ± 1	

[a] $[Ni^{III}(CN)_4(H_2O)_2^-] = 3 \times 10^{-5}$ M; $[H^+] = 10$ mM; $\mu = 0.1$ ($NaClO_4$). [b] $[Ni^{III}(CN)_4(H_2O)_2^-] = 3 \times 10^{-5}$ M; $[OH^-] = 5.0$ mM; $\mu = 0.1$ ($NaClO_4$).

Since HOCl acts both as a scavenger of any free HCN and as an efficient oxidant for the quantitative oxidation of $Ni^{II}(CN)_4^{2-}$ to $Ni^{III}(CN)_4(H_2O)_2^-$, we believe that the HOCl preparation gives more reliable values of the observed rate constants (Table III) for the decomposition of $Ni^{III}(CN)_4(H_2O)_2^-$ in acidic solution.

No $Ni^{III}(CN)_4(H_2O)_2^-$ is observed when H_2O_2 is mixed with $Ni^{II}(CN)_4^{2-}$ in acid, despite the favorable difference in potential (0.61 V at standard conditions) for this reaction. On the other hand, the rate of loss of $Ni^{III}(CN)_4(H_2O)_2^-$ increases when hydrogen peroxide is present (Table VII). A second-order rate constant of (6 ± 1) × 10^2 M^{-1} s^{-1} is found when H_2O_2 acts as a reducing agent. The reduction potential for the O_2/H_2O_2 couple[24] is 0.695 V, which is 0.45 V lower than the $E°$ value for the $Ni^{III}(CN)_4(H_2O)_2^-/Ni^{II}(CN)_4^{2-}$ couple. The possibility of the catalytic decomposition of H_2O_2 by $Ni^{II}(CN)_4^{2-}$ is ruled out because no oxygen is released when $Ni^{II}(CN)_4^{2-}$ is added to an acidic 0.1 M H_2O_2 solution (in 0.1 M $HClO_4$).

Kinetics of the Decomposition in Base. In contrast to its relatively slow decomposition in acid, $Ni^{III}(CN)_4(H_2O)_2^-$ is very unstable with regard to redox decomposition in base, and the reaction is pH dependent (Table III). Its half-life decreases from 28 min at pH 2 to 1.5 s at pH 11.5. The $Ni^{III}(CN)_4(H_2O)_2^-$ decomposition is faster with a HOCl-generated sample than with a bulk-electrolysis-generated sample. The decomposition rate depends on the OCl^- concentration in base, probably due to the oxidation of OCl^- by $Ni^{III}(CN)_4(H_2O)_2^-$. A possible product of the reaction is chlorite, because the standard reduction potential of the ClO_2^-/ClO^- couple in base (0.68 V vs NHE)[24] would favor the reaction. Therefore, the observed rate constants for the decomposition of $Ni^{III}(CN)_4(H_2O)_2^-$ in basic solution are considered more reliable for samples prepared by bulk electrolysis.

Temperature Dependence of the Decomposition in Acid and Base. The temperature dependence of the decomposition of $Ni^{III}(CN)_4(H_2O)_2^-$ in both acid and base and the activation parameters are given in Table VIII. The value for ΔH^* for the decomposition of $Ni^{III}(CN)_4(H_2O)_2^-$ in acid (108 ± 4 kJ mol^{-1}) is higher than

(22) (a) Martell, A. E.; Smith, R. M. *Critical Stability Constants*; Plenum: New York: 1976; Vol. 4. (b) *Ibid.*, 1975; Vol. 2.
(23) Lister, M. W. *Can. J. Chem.* **1956**, *34*, 489–501.
(24) Bard, A. J.; Parsons, R.; Jordan, J. *Standard Potentials in Aqueous Solution*; Dekker: New York, 1985.

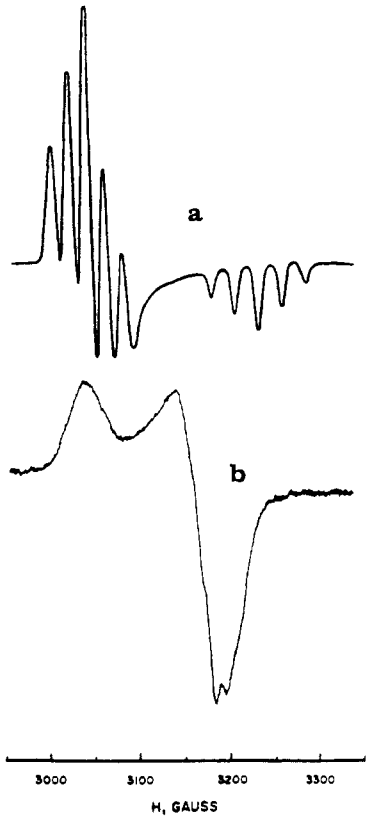

Figure 2. EPR spectra of pyridine and 2,2′-bipyridine complexes with $Ni^{III}(CN)_4^-$ in frozen aqueous samples at −150 °C, μ = 0.1 ($NaClO_4$), and 9.086 GHz: (a) *trans*-$Ni^{III}(CN)_4(py)_2^-$ formed from 2.5×10^{-4} M $Ni^{III}(CN)_4(H_2O)_2^-$ and 5.0×10^{-2} M pyridine at pH 5.4; (b) *cis*-$Ni^{III}(CN)_4bpy^-$ formed from 5.0×10^{-4} M $Ni^{III}(CN)_4(H_2O)_2^-$ and 8.0×10^{-3} M bipyridine at pH 5.

the $\Delta H^{\ddagger}$ value in base (95 ± 1 kJ mol^{-1}). However, the $\Delta S^{\ddagger}$ value for the reaction in acid (52 ± 1 J mol^{-1} K^{-1}) is smaller than the $\Delta S^{\ddagger}$ value in base (69 ± 1 J mol^{-1} K^{-1}). The lower activation enthalpy and the higher positive activation entropy facilitate the base decomposition of $Ni^{III}(CN)_4(H_2O)_2^-$. The positive activation entropies under both conditions indicate that the $Ni^{III}(CN)_4(H_2O)_2^-$ decomposition has a transition state that generates more molecules. It is conceivable that the transition state is $Ni^{II}(CN)_3(^{\bullet}CN)^-$ in acid. Since the Ni^{II} complex prefers to maintain a square-planar configuration, the two axial water molecules on $Ni^{III}(CN)_4(H_2O)_2^-$ could be released in the transition state to give a positive activation entropy. Generally, release of one water molecule from the axial position would generate an entropy increase of 29 J mol^{-1} K^{-1}.[25] The loss of two axial waters in the decomposition of $Ni^{III}(CN)_4(H_2O)_2^-$ would produce an activation entropy of 58 J mol^{-1} K^{-1}, which is close to the experimental value. In base, an attack of OH^- on one of the coordinated cyanides could facilitate the electron transfer from the cyanide to the Ni to give a transition state: $Ni^{II}(CN)_3(HOCN^{\bullet})^{2-}$. The highly solvated hydroxide ion must release water molecules while it attacks $Ni^{III}(CN)_4(H_2O)_2^-$. These additional water molecules released in the transition state could counterbalance the uptake of a hydroxide ion and result in an increase of activation entropy in base.

Mixed-Ligand Complexes. Frozen-Solution EPR Spectra. A variety of ligands will replace both axial waters of $Ni^{III}(CN)_4(H_2O)_2^-$, and these mixed-ligand complexes can be observed by EPR in frozen aqueous solution. These trans-axial complexes are characterized by spectral shifts in their frozen EPR spectra (Table I). Azide ion forms a deep blue mixed cyano complex, whereas the other mixed species are colorless. The EPR spectrum for the bis-substituted-pyridine (py) complex, $Ni^{III}(CN)_4(py)_2^-$ (Figure 2a), as well as mixed cyano complexes of imidazole (imid), NH_3,[1] and acetonitrile (CH_3CN) in frozen aqueous solution shows intense hyperfine splitting in both the $g_{\parallel}$ and $g_{\perp}$ regions. Similar splitting of both $g_{\perp}$ and $g_{\parallel}$ is observed for the $Ni^{III}(cyclam)(NCS)_2^+$ complex.[20] With the exception of bpy (2,2′-bipyridine), all the complexes listed in Table I have tetragonally elongated geometries with $g_{\perp} > g_{\parallel}$. The complexes show a characteristic shift of $g_{\perp}$ to smaller values, and the shift is greater with stronger axial donors. The shift in $g_{\perp}$ is reflected in g_{av}, which decreases in the order

$$CN^- < NH_3 < \text{imid} < N_3^- < \text{py} < CH_3CN < Cl^- < NCO^- < H_2O$$

As the strength of the axial coordination increases, the complex becomes less tetragonally distorted. For the cyanate ion substituted complex, the complex was frozen at pH 5 and the frozen-solution EPR spectrum indicates N-bonded cyanate ions, which are weaker axial donors than either Cl^- or CH_3CN and stronger than H_2O.

The hyperfine splitting in the $g_{\parallel}$ region (A_{zz}) for complexes in Table I that contain nitrogen axial donors increases in the order

$$\text{imid } (sp^2) > \text{py } (sp^2) > CH_3CN \text{ (sp)} \simeq NH_3 \text{ (sp}^3\text{)} > NCO^- \text{ (sp)} > N_3^- \text{ (sp}^2\text{)}$$

due to increased interaction of the axial donor orbital with the nickel d_{z^2} orbital, which contains the unpaired electron. Several factors influence this orbital interaction. These include overall ligand donor strength, s character of the ligand orbital, and electrostatic effects between the ligand group and the Ni(III) complex. Cyanate and azide ions exhibit the lowest A_{zz} values among nitrogen donors. These lower A_{zz} values are attributed to weaker donor strength and to electrostatic repulsion between these negatively charged ligands and $Ni^{III}(CN)_4(H_2O)_2^-$. However, cyanate ion has a greater A_{zz} value compared to azide due to its greater ligand orbital s character. For imidazole and pyridine complexes, both axial groups are sp^2 hybridized and therefore the difference in A_{zz} values is attributed to donor strength of the axial group (g_{av} values). Of the factors mentioned that affect the hyperfine coupling in $g_{\parallel}$, electrostatic effects and ligand orbital s character appear to predominate. Thus, azide ion, in spite of being a moderate donor, shows limited hyperfine coupling due to its negative charge and intermediate s character.

A similar approach can be used to explain the relative hyperfine splitting observed in the $g_{\perp}$ region (A_{xx}, A_{yy}) for the same nitrogen donors. In this instance, it is the interaction between the x and y components of the d_{z^2} orbital (i.e. $d_{z^2-x^2-y^2}$) and the axial donor's nuclear spin. Hence imidazole, pyridine, CH_3CN, and NH_3, which show extensive splitting in $g_{\parallel}$, also show extensive splitting in $g_{\perp}$.

The addition of 2,2′-bipyridine (bpy) to a solution of $Ni^{III}(CN)_4(H_2O)_2^-$ followed by rapid freezing leads to a mixed bpy–cyano complex. The EPR spectrum (Figure 2b) indicates that this cyano complex is tetragonally compressed, with $g_{\parallel} > g_{\perp}$.[17] This places the unpaired electron in the $d_{x^2-y^2}$ orbital. The splitting observed in the $g_{\perp}$ region indicates two equatorial nitrogen donors. A mono complex, $Ni^{III}(CN)_4(bpy)^-$, in which bpy is chelated in the equatorial plane, is proposed (structure II). The long equatorial

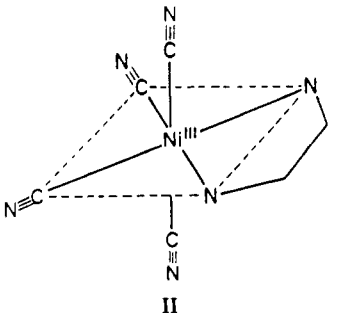

II

N⌒N = bpy

axes each consist of a pyridine nitrogen donor and cyanide donor, while the short axis is the trans CN^- axis.

Room-Temperature EPR Spectra and Stability Constants. Several of the complexes observed in frozen-solution EPR studies (Table I) are also formed at room temperature. Both imidazole

(25) Koval, C. A.; Margerum, D. W. *Inorg. Chem.* **1981**, *20*, 2311–2318.

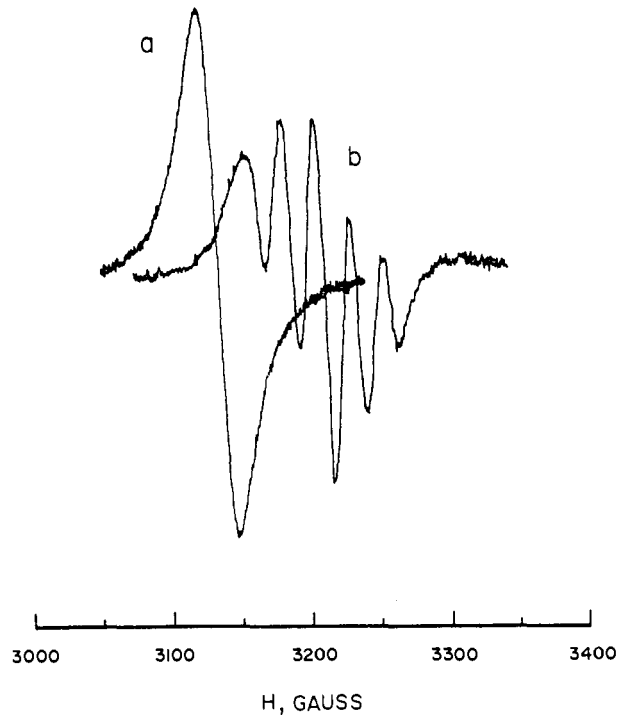

Figure 3. Aqueous room-temperature EPR spectra of nickel(III) cyano complexes at 9.40 GHz and $\mu = 0.1$ ($NaClO_4$): (a) 1×10^{-3} M $Ni(CN)_4(H_2O)_2^-$ at pH 2; (b) 1×10^{-3} M $Ni(CN)_4(H_2O)_2^-$ with 2.5×10^{-2} M imidazole at pH 7.2.

and pyridine give EPR spectra at room temperature that have intense five-line N-hyperfine splittings. Figure 3 compares the aqueous room-temperature EPR spectra of $Ni^{III}(CN)_4(H_2O)_2^-$ and of the fully formed bis(imidazole) complex, $Ni^{III}(CN)_4(imid)_2^-$. The hyperfine splitting for $Ni^{III}(CN)_4(imid)_2^-$ is similar to that observed in the frozen spectrum. The estimated stability constant (β_2) for this complex is greater than 2×10^5 M^{-2}. A similar five-line room-temperature EPR spectrum is observed for the bis(pyridine) complex at high pyridine concentration ([Ni(III) $\simeq$ 0.3 mM, $[py]_T$ = 50 mM, pH 5.4). At lower pyridine concentration ([Ni(III) $\simeq$ 0.3 mM, $[py]_T$ = 0.50 mM, pH 5.4), the EPR spectrum exhibits three-line N-hyperfine splitting, which corresponds to the mono(pyridine) complex, $Ni^{III}(CN)_4(py)(H_2O)^-$. The stepwise equilibrium constants for the formation of $Ni^{III}(CN)_4(py)(H_2O)^-$ and $Ni^{III}(CN)_4(py)_2^-$ are estimated as 10^5 M^{-1} and 4×10^2 M^{-1} ($\mu = 0.1$, 22 °C), respectively. The equilibrium constant for the mono complex is much larger than the value of 40–60 M^{-1} determined for the formation of mono(pyridine)-substituted nickel(III) peptide complexes.[5] This indicates stronger axial coordination for pyridine in $Ni^{III}(CN)_4(py)(H_2O)^-$.

Not all of the complexes that are observed by EPR spectroscopy in frozen aqueous samples are formed in appreciable quantities at room temperature. Even in 0.5 M Cl^-, the aqueous solution of $Ni^{III}(CN)_4(H_2O)_2^-$ provides no EPR evidence of chloride complexation, while the frozen solution with 3.5×10^{-2} M Cl^- (Table I) gives an EPR spectrum that agrees with the spectrum of the $Ni^{III}(CN)_4Cl_2^{3-}$ complex observed in NaCl crystals.[26-28] The inability to observe Cl^- coordination at room temperature, while the bis(chloro) complex is easily formed in the frozen state, reflects equilibrium shifts caused by the freezing process. Earlier work[5] with nickel(III) peptide complexes showed that the freezing process leads to preferential axial coordination of Cl^- or NH_3 to form species that were not observed in room-temperature solution.

(26) Jain, S. C.; Reddy, K. V.; Gupta, C. L.; Reddy, T. Rs. *Chem. Phys. Lett.* **1973**, *21*, 150–152.
(27) Reddy, K. V.; Reddy, T. Rs.; Jain, S. C. *J. Magn. Reson.* **1974**, *16*, 87–94.
(28) Jain, S. C.; Reddy, K. V.; Reddy, T. Rs. *J. Chem. Phys.* **1975**, *62*, 4366–4372.

Table IX. Comparison of Decomposition Rate Constants for $Ni^{III}(CN)_4(H_2O)_2^-$ and Mixed-Ligand Complexes of $Ni^{III}(CN)_4(H_2O)_2^-$ [a]

ligand	[L], M[b]	−log [H^+]	$10^3 k_{obsd}$, s^{-1}
pyridine[c]	0	5.43	6.4 ± 0.7
	3.0×10^{-4}	5.43	11 ± 1
	3.0×10^{-2}	5.43	7.6 ± 0.8
	4.5×10^{-2}	6.23	6.5 ± 0.7
imidazole[c]	0	7.22	3.3 ± 0.2
	3.0×10^{-2}	7.22	6.7 ± 0.3
CH_3CN[d]	0	2.00	1.1 ± 0.3
	2.5	2.00	2.21 ± 0.03
	5.0	2.00	2.46 ± 0.06

[a] $\mu = 0.1$ ($NaClO_4$). [b] Unprotonated ligands; $pK_a(Hpy^+) = 5.24$ ($\mu = 0.1$); $pK_a(Himid^+) = 7.03$ ($\mu = 0.16$); ref 22b. [c] $[Ni^{III}(CN)_4(H_2O)_2^-] = 2 \times 10^{-4}$ M; 22 °C. [d] $[Ni^{III}(CN)_4(H_2O)_2^-] = 3 \times 10^{-5}$ M; 25.0 °C.

For 0.5 mM $Ni^{III}(CN)_4(H_2O)_2^-$ in the presence of CH_3CN in 0.01 M $HClO_4$, the room-temperature EPR results show slight evidence for a mono(acetonitrile) complex (three peaks) in 9.5 M CH_3CN. A similar room-temperature EPR spectrum is observed in 5.0 M CH_3CN with less pronounced splitting. UV–vis spectra taken at 9.5 M CH_3CN and 0.05 mM $Ni^{III}(CN)_4(H_2O)_2^-$ show no unusual spectral features that might indicate CH_3CN coordination. In contrast, the EPR spectrum of the frozen solution shows intense five-line N-hyperfine splitting in both $g_\perp$ and $g_\parallel$ due to $Ni^{III}(CN)_4(NCCH_3)_2^-$ at 9.5 M CH_3CN. It appears that the mono(acetonitrile) complex, $Ni^{III}(CN)_4(NCCH_3)(H_2O)^-$, is not fully formed at room temperature under the conditions listed above. Rather, there is a mixture of species that includes $Ni^{III}(CN)_4(H_2O)_2^-$ and $Ni^{III}(CN)_4(NCCH_3)(H_2O)^-$: The intense splitting observed in the frozen spectrum (five lines) from the bis complex again signifies a distortion in the equilibrium caused by the freezing process.

Decomposition Kinetics of Mixed-Ligand Complexes. The kinetic stability of tetracyanonickelate(III) in the presence of pyridine and imidazole is not enhanced compared to the decomposition of $Ni^{III}(CN)_4(H_2O)_2^-$ (Table IX). In fact, when $Ni^{III}(CN)_4(py)(H_2O)^-$ is the predominant species, the decomposition is nearly twice as fast. At higher pyridine concentration, where $Ni^{III}(CN)_4(py)_2^-$ is the major species, the decomposition rate is the same as $Ni^{III}(CN)_4(H_2O)_2^-$. Under conditions where $Ni^{III}(CN)_4(imid)_2^-$ is the predominant species (3.0×10^{-2} M imidazole) the decomposition rate is twice as fast as the $Ni^{III}(CN)_4(H_2O)_2^-$ decomposition rate.

An increase in decomposition rate also occurs through the addition of CH_3CN to $Ni^{III}(CN)_4(H_2O)_2^-$ (Table IX). The rate observed in 2.5 M CH_3CN is approximately twice that of $Ni^{III}(CN)_4(H_2O)_2^-$ without CH_3CN. As mentioned previously, room-temperature EPR spectra gave evidence for the presence of a mono(acetonitrile)-substituted $Ni^{III}(CN)_4(H_2O)_2^-$ complex in 5.0 M CH_3CN. The increase in decomposition rate observed in the same CH_3CN concentration range is similar to that seen with the pyridine and imidazole complexes. Hence, the increase in rate is probably caused by the presence of $Ni^{III}(CN)_4(NCCH_3)(H_2O)^-$, which decomposes at a faster rate than $Ni^{III}(CN)_4(H_2O)_2^-$.

For complexes of pyridine, imidazole, and CH_3CN, oxidation of these coordinated groups is unlikely. Rather, the pathway for decomposition is presumed to proceed by oxidation of the cyanide, as in the case of $Ni^{III}(CN)_4(H_2O)_2^-$. These strong axial donors cause an increase in the decomposition rate.

$Ni^{III}(CN)_6^{3-}$ and Its Dynamic Jahn–Teller Distortion. A hexacyano complex forms when excess CN^- is added, and an anisotropic EPR spectrum at −220 °C is observed, which indicates a tetragonally elongated complex (Figure 4). There is a large shift of $g_\perp$ from 2.198 with two axial H_2O molecules to 2.081 with two axial CN^- ions coordinated. Upon warming of the sample to −150 °C, a new signal appears between $g_\perp$ and $g_\parallel$ (Figure 5). Further warming leads to a gradual loss of the anisotropic signal, and a new isotropic signal forms at $g_{av} = {}^1/_3(2g_\perp + g_\parallel) = 2.056$

Figure 4. Frozen-solution EPR spectrum of the $Ni^{III}(CN)_6^{3-}$ ion at −220 °C and 9.08 GHz.

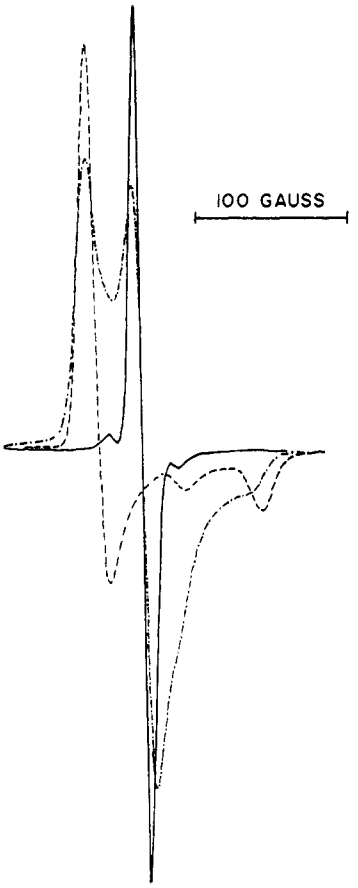

Figure 5. Temperature-variable frozen-solution EPR spectra of $Ni^{III}(CN)_6^{3-}$: (---) −150 °C; (-·-) −60 °C; (—) −35 °C.

(−35 °C). This change is reversible with temperature.[1] The small satellites observed on the isotropic signal are due to the natural abundance of $^{13}CN^-$. This isotropic signal is due to a dynamic Jahn–Teller distortion in which all of the cyanides become equivalent due to vibrational interchange.

Figure 6 shows a cross section of the adiabatic potential energy surface ("Mexican hat" model)[29-31] corresponding to elongation

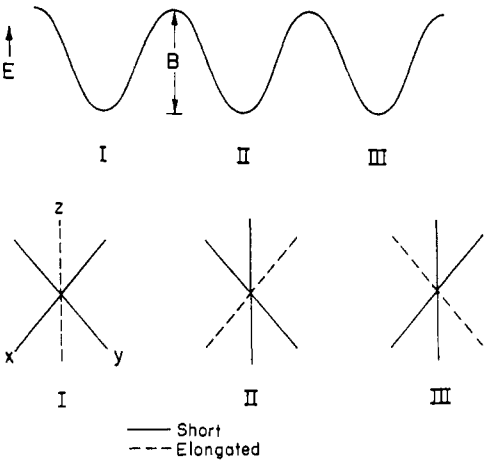

Figure 6. Cross section of adiabatic potential well for the $Ni^{III}(CN)_6^{3-}$ ion.

of each of the equivalent axes of $Ni(CN)_6^{3-}$. When the thermal energy, kT, is less than the barrier-wall energy, B, a static Jahn–Teller distortion is observed, which results in a tetragonally elongated EPR spectrum. When $kT > B$, the axes dynamically interconvert and a pseudooctahedral EPR spectrum is seen. This results in the high-temperature isotropic spectrum.

This is similar to what is observed for the d^7 cobalt(II) hexanitro complexes[32-34] and nickel(III) hexafluoro complexes.[31,35] Several d^9 copper(II) complexes[31,32] have also been shown to undergo temperature-dependent EPR spectral changes from anisotropic to isotropic signals. These effects have all been explained as arising from a vibrational interchange mechanism, where the equivalent elongated axis vibrationally interconverts among the three orthogonal orientations. Transitions from static to dynamic Jahn–Teller distortions have been shown for other nickel(III) complexes.[36-38]

This interconversion of the axes is dramatically shown by the EPR spectrum of the isotopically enriched cyano complex, $Ni(^{13}CN)_6^{3-}$, reported earlier.[1] Equatorial $^{13}CN^-$ is "EPR silent" in tetragonally elongated nickel(III) complexes, while intense $g_\perp$ and $g_\parallel$ splitting is observed for axial $^{13}CN^-$. The spectrum at −190 °C shows a 1:2:1 triplet in both g regions, which indicates two elongated $^{13}CN^-$'s along the z axis. The spectrum at −35 °C shows a seven-line 1:6:15:20:15:6:1 splitting pattern due to six equivalent $^{13}CN^-$. This is attributed to rapid interchange of the elongated axis.

UV Spectral Evidence of $Ni^{III}(CN)_5^{2-}$ or $Ni^{III}(CN)_6^{3-}$. The base decomposition of $Ni^{III}(CN)_4(H_2O)_2^-$ is slower when excess cyanide is present in the solution, and there are immediate changes in the UV spectra upon the addition of cyanide. Figure 7a shows the first spectrum taken 20 s after the $Ni^{III}(CN)_4(H_2O)_2^-$ solution (in 0.001 M H^+) is mixed (1:1) with 0, 0.20, and 0.50 M CN^- (in 0.011 M OH^-) at 1 °C, respectively. Without added cyanide, very little $Ni^{III}(CN)_4(H_2O)_2^-$ is left 20 s after the mixing and the observed spectrum is primarily due to $Ni^{II}(CN)_4^{2-}$. On the other hand, there are substantial amounts of Ni(III) left in the solutions with excess cyanide as shown in Figure 7a by the absorption where $Ni^{II}(CN)_4^{2-}$ does not absorb. The spectral differences between the first spectrum (for 0.10 and 0.25 M CN^-) and the final

(29) Ammeter, J. H.; Burgi, H. B.; Gamp, E.; Meyer-Sandrin, V.; Jensen, W. P. *Inorg. Chem.* **1979**, *18*, 733–750.
(30) Hathaway, B. J. *Struct. Bonding (Berlin)* **1984**, *57*, 55–118.
(31) Reinen, D.; Friebel, C. *Struct. Bonding (Berlin)* **1979**, *37*, 1–60.
(32) Elliott, H.; Hathaway, B. J.; Slade, R. C. *Inorg. Chem.* **1966**, *5*, 669–677.
(33) Bertrand, J. A.; Carpenter, D. A.; Kalyanaraman, A. R. *Inorg. Chim. Acta* **1971**, *5*, 113–114.
(34) Backes, Von G.; Reinen, D. *Z. Anorg. Allg. Chem.* **1975**, *418*, 217–228.
(35) Reinen, D.; Friebel, C.; Propach, V. *Z. Anorg. Allg. Chem.* **1974**, *408*, 187–207.
(36) Shen, L. N.; Estle, T. L. *J. Phys. C* **1979**, *12*, 2103–2118.
(37) Shen, L. N.; Estle, T. L. *J. Phys. C* **1979**, *12*, 2119–2132.
(38) Bates, C. A.; Wardlaw, R. S. *J. Phys. C* **1979**, *12*, 2133–2142.

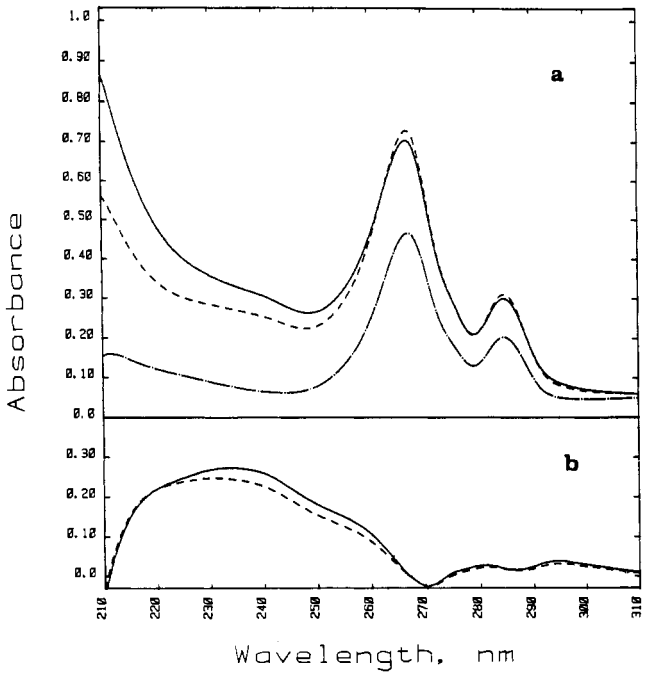

Figure 7. (a) Absorption spectra (1-cm cell, 1 °C, μ = 0.5) taken 20 s after 1 × 10^{-4} M $Ni^{III}(CN)_4(H_2O)_2^-$ in 0.001 M $HClO_4$ was mixed with an equal volume of 0.011 M NaOH (-·-) and with 0.011 M NaOH that contained (---) 0.20 M and (—) 0.50 M NaCN. (b) Spectral difference (for 0.1 and 0.25 M CN^-, after mixing) between spectra taken at 20 s and those taken after the reactions were complete.

Table X. Effect of Cyanide on the Base Decomposition Rate Constant of $Ni^{III}(CN)_4(H_2O)_2^-$ [a]

[CN^-], M	k_{obsd}, s^{-1}	[CN^-], M	k_{obsd}, s^{-1}
0	0.47 ± 0.02	0.15	0.29 ± 0.02
0.025	0.40 ± 0.01	0.20	0.32 ± 0.04
0.050	0.34 ± 0.01	0.25	0.34 ± 0.02
0.10	0.31 ± 0.02	0.50	0.44 ± 0.04

[a] $[Ni^{III}(CN)_4(H_2O)_2^-]$ = 6 × 10^{-5} M; $[OH^-]$ = 5.0 × 10^{-3} M; μ = 1.0 ($NaClO_4$, NaCN); 25.0 °C.

spectrum (after the reaction is complete) are calculated and plotted in Figure 7b. Since $Ni^{II}(CN)_4^{2-}$ is generated as the product during the reaction, the absorbance values at some wavelengths are higher in the final spectrum and correction is made to compensate for these changes before the subtraction. The small negative value at 270 nm in Figure 7b is due to some imperfect compensation. An evident feature from both of the spectral differences in Figure 7b is that a peak appears at 235 nm. Since $Ni^{II}(CN)_4^{2-}$ has negligible absorption and $Ni^{III}(CN)_4(H_2O)_2^-$ has a spectral minimum in this spectral region (220–240 nm), the appearance of the peak at 235 nm indicates a new species. We believe that the new species is either the pentacyano or the hexacyano complex of nickel(III). In frozen aqueous solutions $Ni^{III}(CN)_6^{3-}$ is fully formed under these conditions.

Kinetics of Base Decomposition in the Presence of Cyanide. The kinetics of the base decomposition of $Ni^{III}(CN)_4(H_2O)_2^-$ have a complex cyanide dependence. As shown in Table X for 5.0 × 10^{-3} M OH^- and μ = 1.0, the rate of the reaction decreases when the cyanide concentration increases, in contrast to the fact that in acid excess HCN accelerates the decomposition of $Ni^{III}(CN)_4(H_2O)_2^-$. The rate reaches a minimum at [CN^-] = 0.15 M and then increases again with increasing cyanide concentration. A possible explanation of the kinetic behavior is that a pentacyano complex of nickel(III) forms, which is slower to decompose than the tetracyano and hexacyano complexes (Scheme I). Under pseudo-first-order conditions, the observed rate constant of the reaction is defined in eq 3, where k_1 = 0.47 ± 0.02 s^{-1}, k_2 and k_3 are

$$k_{obsd} = \frac{k_1 + k_2K_1[CN^-] + k_3K_1K_2[CN^-]^2}{1 + K_1[CN^-] + K_1K_2[CN^-]^2} \quad (3)$$

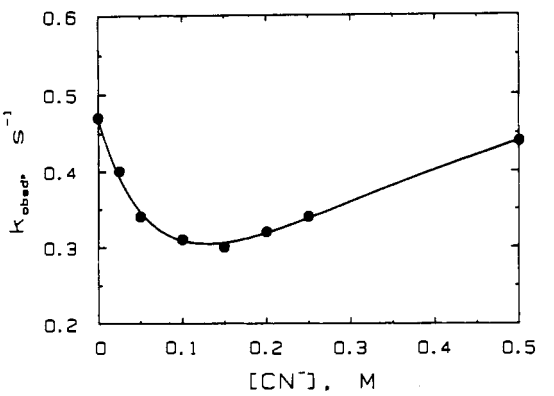

Figure 8. Rate constants of the base decomposition of Ni(III) cyano complex at different cyanide concentrations. Conditions: $[Ni]_T$ = 6 × 10^{-5} M; oxidized at 1.20 V (vs Ag/AgCl); $[OH^-]$ = 5 × 10^{-3} M; μ = 0.5; 25.0 °C. The reaction was monitored at 234 nm. The solid line is a fit of eq 4 or 5 to the data.

Scheme I

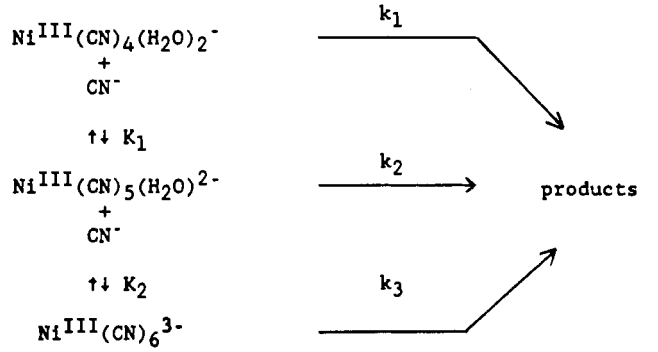

Scheme II

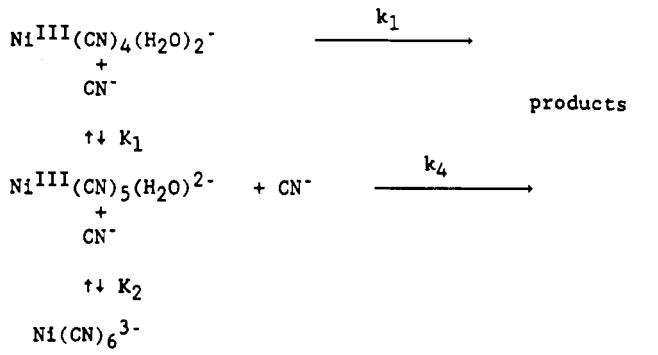

decomposition rate constants, and K_1 and K_2 are the formation equilibrium constants for the pentacyano and hexacyano complexes, respectively. A nonlinear fit of eq 3 to the data listed in Table X yields k_2 = −0.2 ± 0.5. This indicates that the pentacyano complex is relatively stable and that its decomposition can be neglected. Using k_2 = 0 results in eq 4. The nonlinear fit of eq

$$k_{obsd} = \frac{k_1 + k_3K_1K_2[CN^-]^2}{1 + K_1[CN^-] + K_1K_2[CN^-]^2} \quad (4)$$

4 to the data is shown in Figure 8, and the constants obtained are k_3 = 0.82 ± 0.02 s^{-1}, K_1 = 8.5 ± 0.7 M^{-1}, and K_2 = 2.3 ± 0.1 M^{-1}.

Another possible mechanism is given in Scheme II, where once again pentacyano and hexacyano complexes are formed, but the pentacyano complex decomposes by reaction with free CN^- and the hexacyano complex does not have an appreciable rate of decomposition. This gives the rate constant expression in eq 5,

$$k_{obsd} = \frac{k_1 + k_4K_1[CN^-]^2}{1 + K_1[CN^-] + K_1K_2[CN^-]^2} \quad (5)$$

which has the same cyanide dependence and the same values of

K_1 and K_2 as in eq 4. The value of k_4 is 1.9 M^{-1} s^{-1}. Both schemes indicate that pentacyano and hexacyano complexes exist in basic aqueous solution and that their stability constants are not very large.

Acknowledgment. This work was supported by National Institutes of Health Grant GM-12152 and by National Science Foundation Grants CHE-8616666 and CHE-8720318.

Registry No. $Ni^{III}(CN)_4(H_2O)_2^-$, 97011-73-9; $Ni^{III}(CN)_6^{3-}$, 97011-80-8; $Ni^{III}(^{13}CN)_4(H_2O)_2^-$, 117226-39-8; $Ni^{III}(CN)_4(NCO)_2^{3-}$, 97011-79-5; $Ni^{III}(CN)_4(Cl)_2^{3-}$, 54003-01-9; $Ni^{III}(NCCH_3)_2^-$, 97011-77-3; $Ni^{III}(py)_2^-$, 97011-76-2; $Ni^{III}(N_3)_2^{3-}$, 97011-78-4; $Ni^{III}(imid)_2^-$, 97011-75-1; $Ni^{III}(bpy)_2^-$, 117226-40-1; $Ni^{II}(CN)_4^{2-}$, 48042-08-6; OCN^-, 661-20-1; HCN, 74-90-8; H_2O_2, 7722-84-1; CN^-, 57-12-5.

Contribution from the Institute for Inorganic Chemistry, University of Witten/Herdecke, Stockumerstrasse 10, 5810 Witten, Federal Republic of Germany

Solvent Dependence of the Activation Parameters for the Solvolysis of a Square-Planar Complex, (Pyridine)(pentamethyldiethylenetriamine)palladium(II)

M. Kotowski,[1a] S. Begum,[1a,b] J. G. Leipoldt,[1c] and R. van Eldik*

Received April 27, 1988

The solvolysis reaction of $Pd(Me_5dien)py^{2+}$ was studied as a function of temperature and pressure in the solvents H_2O, MeOH, EtOH, Me_2SO, DMF, and MeCN in order to gain insight into the solvent dependence of this process. The selected system involves the release of a neutral ligand, which reduces possible contributions from electrostriction and thus enables an estimation of the intrinsic component of the activation parameters. The activation entropy is negative throughout, and the activation volume varies between 0 and −6 cm^3 mol^{-1}, characteristic for an associative substitution process.

Introduction

We have a longstanding interest in the substitution mechanisms of sterically-hindered square-planar complexes of Pt(II) and Pd(II).[2] These studies have emphasized the significance of spontaneous solvolysis reactions and their integrated role in the substitution behavior of such complexes.[3] For a series of diethylenetriamine (dien) and substituted dien complexes of Pd(II), we demonstrated that although a severe increase in steric hindrance can slow down the solvolysis process in aqueous solution by up to 6 orders of magnitude, it does not affect the fundamental associative nature of the substitution process.[4] For a particular leaving group, vis. Cl^-, the increase in steric hindrance is accompanied by an increase in $\Delta H^{\ddagger}$, whereas $\Delta S^{\ddagger}$ and $\Delta V^{\ddagger}$ remain constant and strongly negative throughout the series of complexes. Later work[5,6] demonstrated that these parameters, especially $\Delta V^{\ddagger}$, depend significantly on the nature of the leaving group. For instance, more negative $\Delta V^{\ddagger}$ values (between −8 and −16 cm^3 mol^{-1}) were found for anionic leaving groups (viz. Cl^-, Br^-, N_3^-, $C_2O_4^{2-}$, CO_3^{2-}), compared to values around −3 cm^3 mol^{-1} for neutral leaving groups such as NH_3 and pyridine (py). This difference was ascribed to solvational changes caused by changes in dipole moment during a square-pyramidal to trigonal-bipyramidal transition in the associative transition state. In this way anionic leaving groups will cause more negative $\Delta V^{\ddagger}$ values, and the value found for neutral leaving groups (viz. −3 cm^3 mol^{-1}) most probably represents the intrinsic volume collapse associated with the overall associative attack of a water molecule.[7] This intrinsic value is significantly smaller than that predicted and observed for associative aquation of octahedral complexes.[8-11]

In order to throw more light on the intimate nature of such solvolysis reactions of square-planar complexes, we have studied the solvent dependence of the activation parameters for the solvolysis of $Pd(Me_5dien)py^{2+}$, i.e., a sterically hindered complex with a neutral leaving group. In general, little is known about the solvent dependence of these parameters,[2] and the data enable us to comment on the intrinsic factors that control these parameters.

Experimental Section

The $[Pd(1,1,4,7,7\text{-}Me_5dien)py](ClO_4)_2$ complex was prepared according to the following procedure. Concentrated pyridine was added to a 10^{-2} M solution of the corresponding aqua complex[12] in a 5:1 ratio, and the reaction mixture was slowly concentrated to a very small volume on a water bath. A light yellow crystalline product separated on cooling the mixture in an ice bath. The product was recrystallized from a 0.1 M aqueous pyridine solution in the same way as described above. The crystals were filtered off, washed with small quantities of ice cold water and ethanol, and dried in a vacuum desiccator. Microanalyses[13] were in good agreement with the theoretically expected values. The complex and its solvolysis products were characterized from their UV-vis spectra recorded on Perkin-Elmer 555 and Shimadzu UV 250 spectrophotometers.

The solvents MeOH, EtOH, Me_2SO, DMF and MeCN were purified and dried according to standard procedures.[14] Chemicals of analytical reagent grade and doubly deionized water were used throughout this study. The reactions at ambient pressure were followed in either the thermostated (±0.1 °C) cell compartment of a Zeiss DMR 10 spectrophotometer or a thermostated (±0.1 °C) Aminco stopped-flow system. At elevated pressure, a thermostated (±0.1 °C) high-pressure cell[15] and a self-constructed high-pressure stopped-flow system[16] were employed. All kinetic measurements were performed under pseudo-first-order conditions and a linearity standard of between 2 and 3 half-lives was set for

(1) (a) Experimental work performed at the Institute for Physical Chemistry, University of Frankfurt, FRG. (b) On leave from the University of Peshawar, Pakistan. (c) On leave from the University of the Orange Free State, South Africa.
(2) Kotowski, M.; van Eldik, R. In *Inorganic High Pressure Chemistry: Kinetics and Mechanisms*; van Eldik, R., Ed.; Elsevier: Amsterdam, 1986; Chapter 4 and references cited therein.
(3) Kotowski, M.; van Eldik, R. *Inorg. Chem.* **1984**, *23*, 3310.
(4) Breet, E. L. J.; van Eldik, R. *Inorg. Chem.* **1984**, *23*, 1865.
(5) Kotowski, M.; van Eldik, R. *Inorg. Chem.* **1986**, *25*, 3896.
(6) Mahal, G.; van Eldik, R. *Inorg. Chem.* **1985**, *24*, 4165.
(7) Helm, L.; Elding, L. J.; Merbach, A. E. *Helv. Chim. Acta* **1984**, *67*, 1453.
(8) Swaddle, T. W. *J. Chem. Soc., Chem. Commun.* **1982**, 832.
(9) Swaddle, T. W.; Mak, M. K. S. *Can. J. Chem.* **1983**, *61*, 473.
(10) Swaddle, T. W. *Inorg. Chem.* **1983**, *22*, 2663.
(11) van Eldik, R. In *Inorganic High Pressure Chemistry: Kinetics and Mechanisms*; van Eldik, R., Ed.; Elsevier: Amsterdam, 1986; Chapters 1 and 3 and references cited therein.
(12) Breet, E. L. J.; van Eldik, R.; Kelm, H. *Polyhedron* **1983**, *2*, 1181.
(13) Hoechst Analytical Laboratory, Frankfurt, FRG.
(14) *Organikum*; VEB Deutscher Verlag der Wissenschaften: Berlin, 1976.
(15) Fleischmann, F. K.; Conze, E. G.; Stranks, D. R.; Kelm, H. *Rev. Sci. Instrum.* **1974**, *45*, 1427.
(16) van Eldik, R.; Palmer, D. A.; Schmidt, R.; Kelm, H. *Inorg. Chim. Acta* **1981**, *50*, 131.

0020-1669/88/1327-4472$01.50/0